Clean Techn Environ Policy (2015) 17:501–513
DOI 10.1007/s10098-014-0807-7

ORIGINAL PAPER

Performance investigation of high-temperature sensible heat thermal energy storage system during charging and discharging cycles

Hakeem Niyas · Likhendra Prasad · P. Muthukumar

Received: 16 March 2014 / Accepted: 13 June 2014 / Published online: 5 July 2014

Abstract This paper presents the thermal modelling and performance predictions of high-temperature sensible heat storage (SHS) models of 50 MJ capacity designed for solar thermal power plant applications in the temperature range of 523–648 K. The SHS unit is a regenerator-type heat exchanger which stores/releases the heat on passing hot/cold heat transfer fluid (HTF) through the tubes embedded into it. A mathematical model of cylindrical configuration with embedded multi-tube is developed employing concrete and cast steel as the storage media. The number of embedded charging/discharging tubes in the storage model is optimized based on the charging time using the finite element method-based simulation tool, COMSOL Multiphysics. Numerically predicted results match well with the data reported in the literature. Thermal performance parameters of SHS bed such as charging/discharging time, energy stored/recovered, charging/discharging energy efficiency and overall efficiency have been evaluated. Axial variations of HTF temperature during charging/discharging cycle are analysed, and the parametric studies are carried out by varying the flow rate of HTF. For cast steel bed, the increase in HTF velocity resulted in the proportional reduction in charging/discharging time, while these effects in concrete were less because of its low thermal conductivity.

Keywords Solar energy · Sensible heat storage · TES · Tube optimization · Efficiency

List of symbols

C_{ps}	Specific heat of solid-state SHSM (J/kg K)
C_{pf}	Specific heat of HTF (J/kg K)
k_s	Thermal conductivity of solid-state SHSM (W/m K)
k_f	Thermal conductivity of HTF (W/m K)
ρ_s	Density of solid-state SHSM (kg/m^3)
ρ_f	Density of HTF (kg/m3)
μ	Dynamic viscosity of HTF (Ns/m^2)
γ	Kinematic viscosity of HTF (mm^2/s)
d	Internal diameter of the charging tubes (m)
D	Diameter of SHS bed (m)
L	Length of SHS bed (m)
n	Number of charging tubes
Q	Heat storage capacity (J)
t	Charging time (s)
T_{ch}	Volume average temperature of SHS bed at the end of charging (K)
T_{ini}	Initial temperature of SHS bed (K)
T_{inlet}	HTF inlet temperature (K)
T_{outlet}	HTF outlet temperature (K)
T_{atm}	Atmospheric temperature (K)
ΔT	Charging temperature range (K)
$\vec{v}$	Velocity of HTF (m/s)
V_r	Volume of solid-state SHSM required (m^3)
V_a	Actual volume of solid-state SHSM including factor of safety (m^3)
m	Mass of solid-state SHSM (kg)
η_{ch}	Charging energy efficiency
η_{disch}	Discharging energy efficiency
$\eta_{overall}$	Overall efficiency

Introduction

Recently, solar energy is accepted as one of the most favourable alternative energy options to the conventional

H. Niyas · L. Prasad · P. Muthukumar (✉)
Department of Mechanical Engineering, Indian Institute of Technology Guwahati, Guwahati 781039, India
e-mail: pmkumar@iitg.ernet.in; pmuthukkumar@yahoo.com

fossil fuels. However, the intermittent availability of solar energy leads to an energy gap between demand and supply, i.e. on sunny days, solar energy collected is usually more than energy required for the direct use. Therefore, the design and development of efficient and economical thermal energy storage (TES) systems are of vital importance. However, only very few solar thermal power plants in the world have employed these TES systems (Gil et al. 2010). Thermal energy can be stored in the form of sensible heat, latent heat and heat of reversible chemical reactions. Presently, liquid media storage is a well-known and commercially adopted technology for high-temperature heat storage applications. Solid media and phase change material (PCM) can be substitutes for liquid media storage system which eliminates high-temperature freezing and also avoids the separation of hot and cold heat transfer fluid (HTF). Though, the energy density of PCMs is higher, sensible heat storage (SHS) scores some advantages when compared to latent heat storage (LHS) at high temperature including simplicity in design and construction, high charging and discharging rates, ease of control and hence lower cost.

Various candidate materials for high-temperature SHS systems have been studied (Khare et al. 2013). The main difficulty in using solid media for SHS is the large size of storage bed. However, this can be minimised by using high heat capacity storage material and allowing high-temperature swing. Transient behaviours of SHS system have been investigated using magnesia as sensible heat storage material (SHSM) and air as HTF (Sragovich 1989). A by-product from potash industry has been tested for its suitability as a SHSM (Miró et al. 2014). Performance evaluation has been carried out using alumina as SHSM and compressed air as HTF (Anderson et al. 2014). Castable ceramic and concrete could be used as SHSM for high-temperature heat storage applications (Tamme et al. 2004). Ceramic and concrete have been investigated for a maximum storage temperature of 663 K and a storage capacity of 350 kW. It was concluded that concrete is the more preferable storage material although ceramic is having 20 % higher-storage capacity and 35 % more conductive (Laing et al. 2006). Concrete and castable ceramic-based storage modules have been reported as low cost (25–30 $ kWh) and durable SHS systems (Nandi et al. 2012). It has been observed that heating the concrete at increased temperatures causes certain reactions and transformations occur due to the presence of voids which influence their thermo-physical properties. The compressive strength decreases by about 20 % on heating the concrete to 673 K (Gil et al. 2010). However, such problems can be minimized by the addition of filler materials such as steel needles and reinforcement to improve the mechanical and thermal strength. After exposure to 10 thermal cycles from ambient temperature to 723 K, concrete bed has maintained more than 50 % of their mechanical properties (John et al. 2011).

Table 1 Thermo-physical properties of HTF at different temperatures

T (°C)	ρ_f (kg/m^3)	C_{pf} (kJ/kg K)	k_f (W/m K)	γ (mm^2/s)	μ (Pa s)
40	860	2.0818	0.1314	20.00	0.017200
100	823	2.3062	0.1238	3.82	0.003144
150	790	2.4932	0.1175	1.75	0.001383
200	755	2.6802	0.1119	0.90	0.000680
250	717	2.8672	0.1049	0.69	0.000495
300	678	3.0542	0.0985	0.50	0.000339

It is seen from the reported works that most of the researchers emphasized on the use of high-temperature concrete as SHSM. However, there is a lack of research works on the optimization of number of charging/discharging tubes used in the solid SHS systems based on the charging/discharging time. Hence, in the present work, the thermal storage performances of solid-state SHS systems are investigated by using a high-conductivity material cast steel and a low-conductivity material concrete. Hi-Tech Therm 60 has been selected as the HTF. Number of charging tubes is optimized based on the charging time of SHS bed using the simulation tool COMSOL Multiphysics. The thermal storage characteristics of the selected SHS models are predicted considering the energy storage capacity as 50 MJ.

Design of sensible heat storage bed

The design of SHS bed includes fixing the diameter of storage bed and charging tubes, number of charging tubes and length of storage bed. The minimum volume of SHSM required for storing 50 MJ is calculated using Eq. 1.

$$Q = \rho_s V_r C_{ps} \Delta T \quad (1)$$

In the present case, charging temperature range has been fixed as 100 K. Concrete and cast steel are selected as SHSM based on the thermo-physical properties (Tian and Zhao 2013), cost effectiveness (Khare et al. 2013; Nandi et al. 2012) and easy availability. Moreover, these storage materials are modular in nature and can easily be extended for higher-storage capacity. The actual volume of SHSM with charging/discharging tubes is estimated using Eq. 2. The diameter and length of storage bed are chosen as 0.60 and 1.20 m for concrete and 0.50 and 0.70 m for cast steel. Tube diameter of 0.0125 m with wall thickness 0.0015 m is selected for both cases. Hi-Tech Therm 60 has been selected as the HTF which flows through the charging/

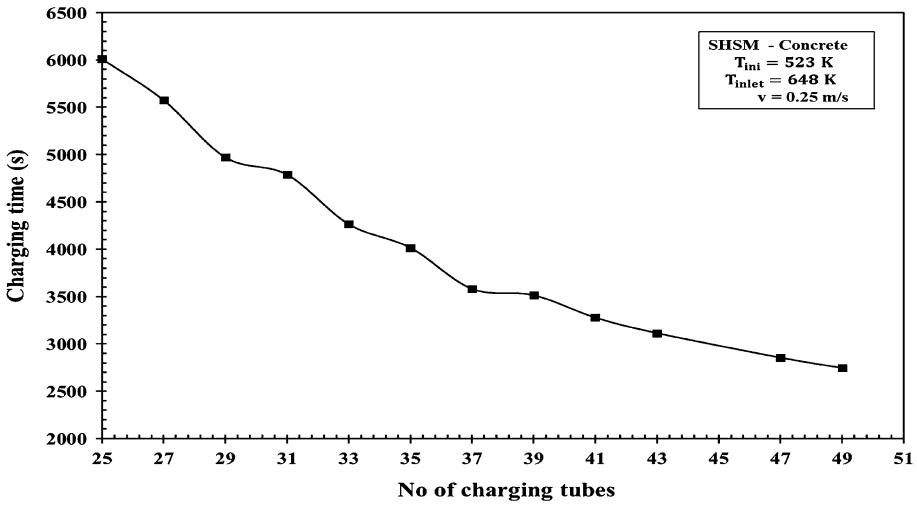

Fig. 1 Optimization of number of charging tubes

Table 2 Thermo-physical properties (Tian and Zhao 2013) and estimated mass of SHSM

S. no	Storage material	ρ_s (kg/m^3)	C_{ps} (J/kg K)	k_s (W/m K)	V_r (m^3)	V_a (m^3)	m (kg)
1	Concrete	2,200	850	1.5	0.267	0.320	705
2	Cast steel	7,800	600	40	0.107	0.128	1,000

discharging tubes exchanging heat with the storage bed. The thermo-physical properties of the HTF at different temperatures have been given in Table 1.

$$V = \left[\frac{\pi}{4}\left(D^2 - \mathrm{nd}^2\right)\right]L \quad (2)$$

Optimization of number of charging tubes in storage bed

Increasing the number of charging tubes reduces the charging time significantly but also reduces the storage capacity marginally. In order to optimize the number of charging tubes, the charging time for different configurations of charging tubes assembly is shown in Fig. 1. It is seen from Fig. 1 that there are three ranges where the charging time does not change significantly with the increase in number of charging tubes. First range falls between 29 and 31 tubes where the difference in charging time is 182 s, second range is between 33 and 35 tubes where the charging time difference is 249 s and third range occurs between 37 and 39 tubes where the difference in charging time is 67 s. It is also seen that after 39 tubes, the charging time decreases continuously with increase in number of charging tubes and no such range is found. Also increasing the number of tubes beyond 49 tubes will not be practically feasible for the given diameter of the SHS bed and also it will lead to manufacturing difficulties. Hence, 37 number of charging tubes is selected for the SHS bed and the estimated mass of SHSM with a factor of 1.2 is given in Table 2.

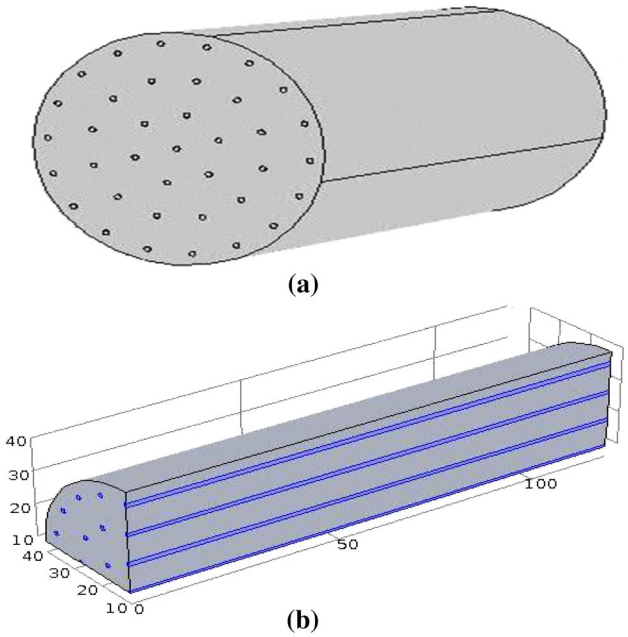

Fig. 2 Schematic diagram of SHS bed **a** physical model **b** sectional view

Thermal modelling of storage bed

The physical model and sectional view of the SHS bed with embedded charging/discharging tubes are illustrated in Fig. 2a, b. The storage unit is a regenerative-type heat exchanger which absorbs/releases heat energy by passing the hot/cold HTF, respectively, through the charging tubes. During the charging/discharging cycle, HTF at high/low temperature, respectively, is supplied to storage bed from one end and it exits from the other end, thus exchanging the heat.

Governing equations

The thermal model of SHS bed is developed based on the following assumptions:

- The inlet velocity profile of HTF is fully developed.
- No axial conduction in HTF.
- The SHSM is isotropic.
- External surface of the SHS bed is adiabatic.

The continuity and Navier–Stokes equations are solved concurrently to simulate the behaviour of the HTF flowing inside the charging tubes of the SHS bed. The energy equation (Eq. 5) is solved using the velocities found from the solutions of Eqs. 3 and 4 to simulate the heat transfer from the HTF to the wall of the pipe. The material derivative term D*T*/D*t* of Eq. 5 takes care the effect of convection heat transfer. The heat conduction equation (Eq. 6) is solved for accounting the heat transfer from the charging tubes to the SHSM. The continuity, Navier–Stokes and energy equations have been solved with an accuracy of 10^{-3} using the PARADISO solver. The simulations have been carried out with a time stepping of 0.1 s.

Fluid flow:

$$\nabla \cdot \vec{v} = 0 \tag{3}$$

$$\rho_f \frac{\mathrm{D}\vec{v}}{\mathrm{D}t} = -\nabla P + \mu \nabla^2 \vec{v} \tag{4}$$

Convection: solid–liquid interface:

$$\rho_{\mathrm{f}}\, C_{\mathrm{pf}} \frac{\mathrm{D}T}{\mathrm{D}t} = k_{\mathrm{s}} \nabla^2 T \tag{5}$$

Conduction: solid region:

$$\rho_{\mathrm{s}} C_{\mathrm{ps}} \frac{\partial T}{\partial t} = k_{\mathrm{s}} \nabla^2 T \tag{6}$$

Initial and boundary conditions

- Initially, there is no flow of HTF through the tubes, and all the domains are at constant temperature of 523 K/623 K during charging/discharging.
- Charging/discharging is initiated by specifying a constant temperature of 648 K/523 K followed by a constant HTF velocity.
- Outer surfaces of the SHS bed are insulated except inlet and outlet.
- There is no slip between the SHS bed and the flow of HTF.

Mesh formation

Free tetrahedral mesh has been adapted to assure that relatively smaller geometries are discretized with sufficient number of elements. The grid size of HTF taken is smaller than the storage bed as it constitutes lesser dimensions when compared to the storage bed. The total number of elements of SHS bed model varies with the configurations of the bed. Meshed geometry of cast steel storage bed is shown in Fig. 3, and total number of elements are given in Table 3 for concrete and cast steel SHS beds.

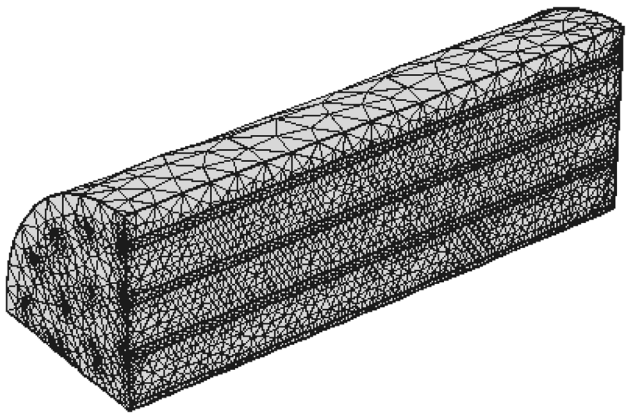

Fig. 3 Meshed geometry of cast steel SHS bed

Table 3 Grid size and number of mesh elements in concrete and cast steel SHS beds

S. no	Storage material	Grid size (cm)				Total number of mesh elements
		Storage bed		HTF		
		Min	Max	Min	Max	
1	Concrete	2.1	9.9	1.2	3.9	95,944
2	Cast steel	1.75	8.25	1	3.25	1,00,405

Performance parameters

Charging time

It is the time taken for the SHS bed's volume average temperature to reach a definite rise in temperature ΔT. When the volume average temperature of SHS bed reaches 623 K, the storage bed is said to be completely charged.

Energy stored

The amount of thermal energy stored in the different storage materials at their corresponding charging times is calculated using Eq. 7. Volume average temperature $T(t)$ is a function of time. As time increases, the temperature also increases during charging through which energy is getting stored in the SHS bed.

$$Q = \rho_s V_a C_{ps}(T(t) - T_{ini}) \quad (7)$$

Charging energy efficiency

This is the efficiency which outlines the capability of SHSM to gain thermal energy from HTF and is primarily based on the first law of thermodynamics. Charging energy efficiency is the ratio of actual energy stored by storage material to maximum energy available as input to storage material (Haller et al. 2009). The charging energy efficiency at the respective charging time is calculated using Eq. 8.

$$\eta_{ch} = \frac{T(t) - T_{ini}}{T_{inlet} - T_{ini}} \quad (8)$$

Discharging time

The time taken by the SHS bed to attain a volume average temperature of 523 K is the complete discharging time of storage bed. But after a certain time, the decrease in storage bed temperature is not significant especially when its temperature approaches to 523 K. Thus, effective discharging time of storage bed is taken as the time till the temperature drop is significant, provided the energy recovered from the storage bed is within the design limit (i.e. at least 50 MJ).

Energy recovered

The amount of thermal energy recovered from storage bed of different materials at the particular discharging time is calculated using Eq. 9. As time increases, the temperature also decreases during discharging through which energy is getting recovered from the SHS bed.

$$Q = \rho_s V_a C_{ps}(T_{ch} - T(t)) \quad (9)$$

Discharging energy efficiency

This efficiency explains the ability of SHSM to exchange heat with the HTF. Discharging energy efficiency is the ratio of actual energy recovered from storage bed to maximum energy that can be recovered. The discharging energy efficiency at the corresponding discharging time is calculated using Eq. 10.

$$\eta_{disch} = \frac{T_{ch} - T(t)}{T_{ch} - T_{inlet}} \quad (10)$$

Overall efficiency

It is the ratio of energy recovered from the storage bed during discharging cycle to the total energy input to storage bed which is given by the Eq. 11. The total energy input is the sum of energy supplied to heat the storage bed from an atmospheric temperature of 303 K to 523 K and energy stored in the bed during charging.

$$\eta_{Overall} = \frac{T_{ch} - T(t)}{T_{ch} - T_{atm}} \quad (11)$$

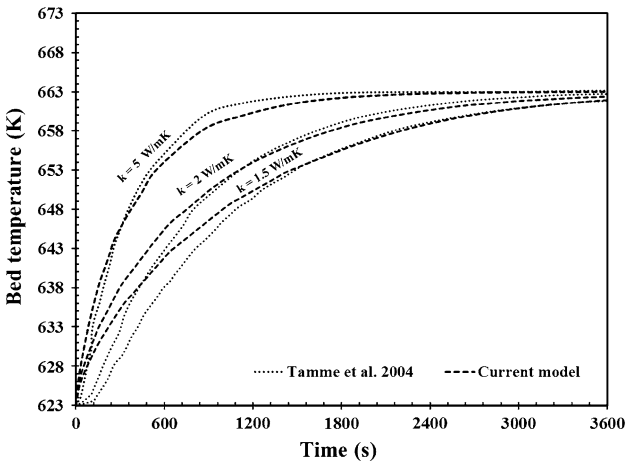

Fig. 4 Validation of the current numerical model of SHS unit

Validation of the numerical model

To validate the current numerical model of SHS unit, the results obtained for the charging time of SHS bed at different values of thermal conductivities have been compared with the charging time reported in Tamme et al. (2004). The physical model chosen for the numerical validation, thermo-physical properties of the SHSM and initial and boundary conditions of the model are taken from Tamme et al. (2004). It is evident from Fig. 4 that the current numerical results showed a good agreement with the results reported in Tamme et al. (2004). There is a small deviation at the initial period of charging time which may be due to the assumption of neglecting axial conduction in HTF.

Results and discussions

Charging time

Charging of storage bed is initiated by supplying HTF through the charging tubes at a high temperature of 648 K. The temperature of storage bed varies with time and space. Charging of concrete and cast steel beds is illustrated in Fig. 5 and 6 through the temperature contours at different intervals of charging cycle. The temperature of storage bed is averaged over the entire bed volume, and hence, it is a function of time only. Variation of volume average bed temperature with time is shown in Fig. 7a for concrete and cast steel beds. It is seen from Fig. 7a that initially, the rise in the volume average temperature of storage beds is rapid and

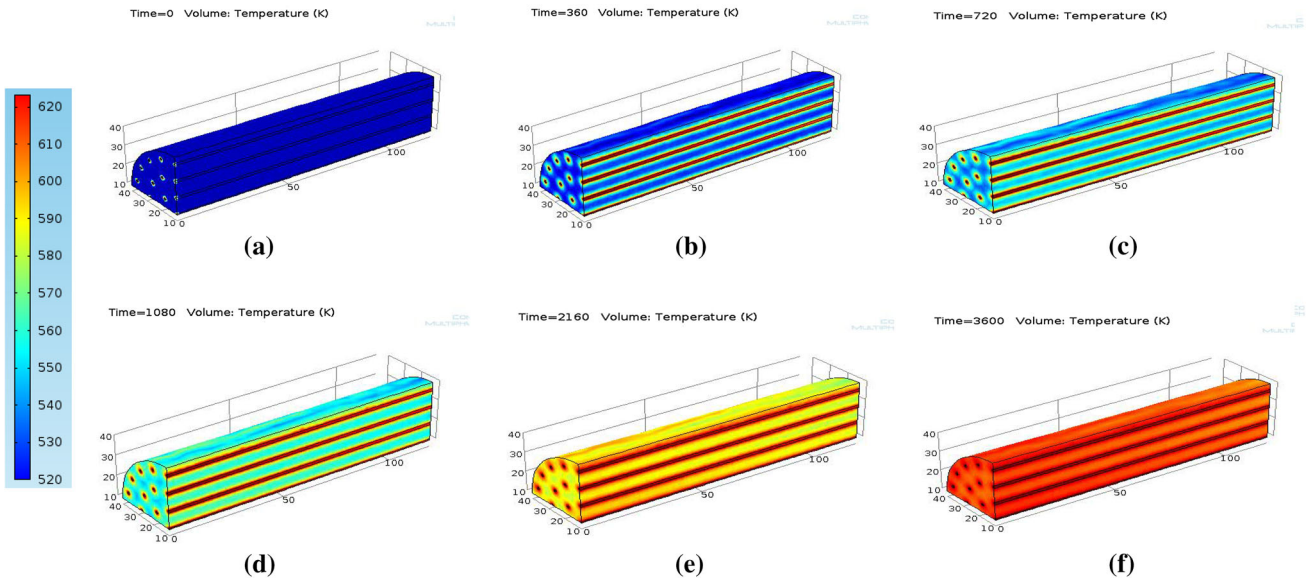

Fig. 5 Temperature contours of concrete SHS bed during charging at different time intervals **a** $t = 0$ s, **b** $t = 360$ s, **c** $t = 720$ s, **d** $t = 1{,}080$ s, **e** $t = 2{,}160$ s, **f** $t = 3{,}600$ s

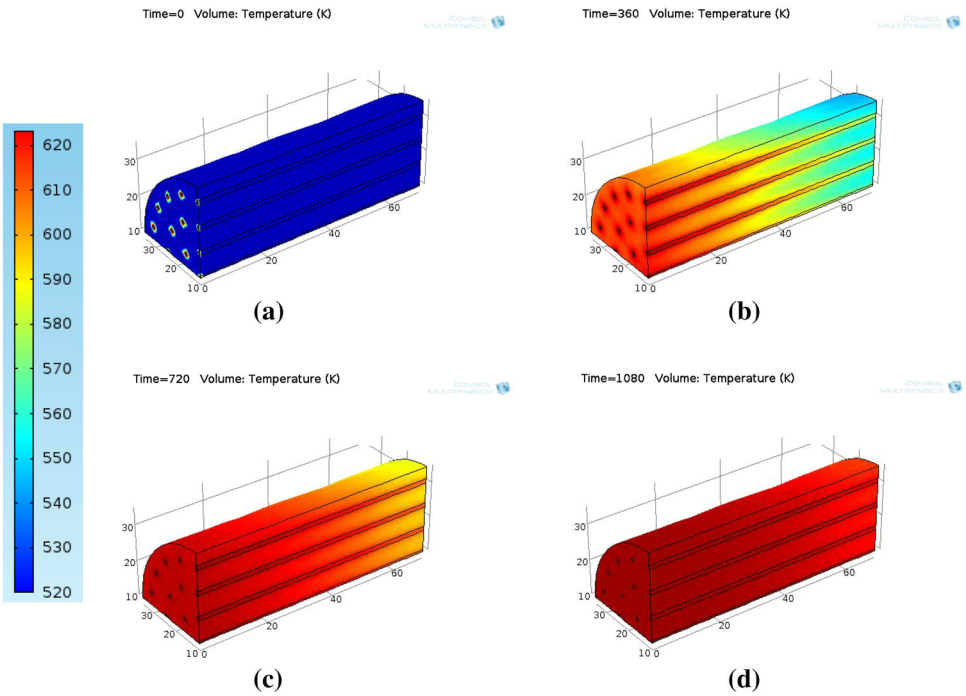

Fig. 6 Temperature contours of cast steel SHS bed during charging at different time intervals, **a** $t = 0$ s, **b** $t = 360$ s, **c** $t = 720$ s, **d** $t = 1{,}080$ s

decreases with time. This is because of higher driving potential available for conduction during initial period of charging cycle, and this driving potential reduces with time as the storage bed gains the heat of HTF. The charging rate of concrete bed is slow as compared to cast steel bed due to the high heat capacity and low thermal conductivity of concrete. The concrete bed takes about 3,650 s for complete charging, whereas cast steel gets completely charged within 683 s.

Thermal energy stored

The TES rates for the concrete and cast steel beds are shown in Fig. 7b. The amount of thermal energy stored in the storage materials at their respective charging times is calculated using Eq. 7. Thermal energy stored in concrete and cast steel beds are 62.39 and 62.85 MJ at their respective charging times.

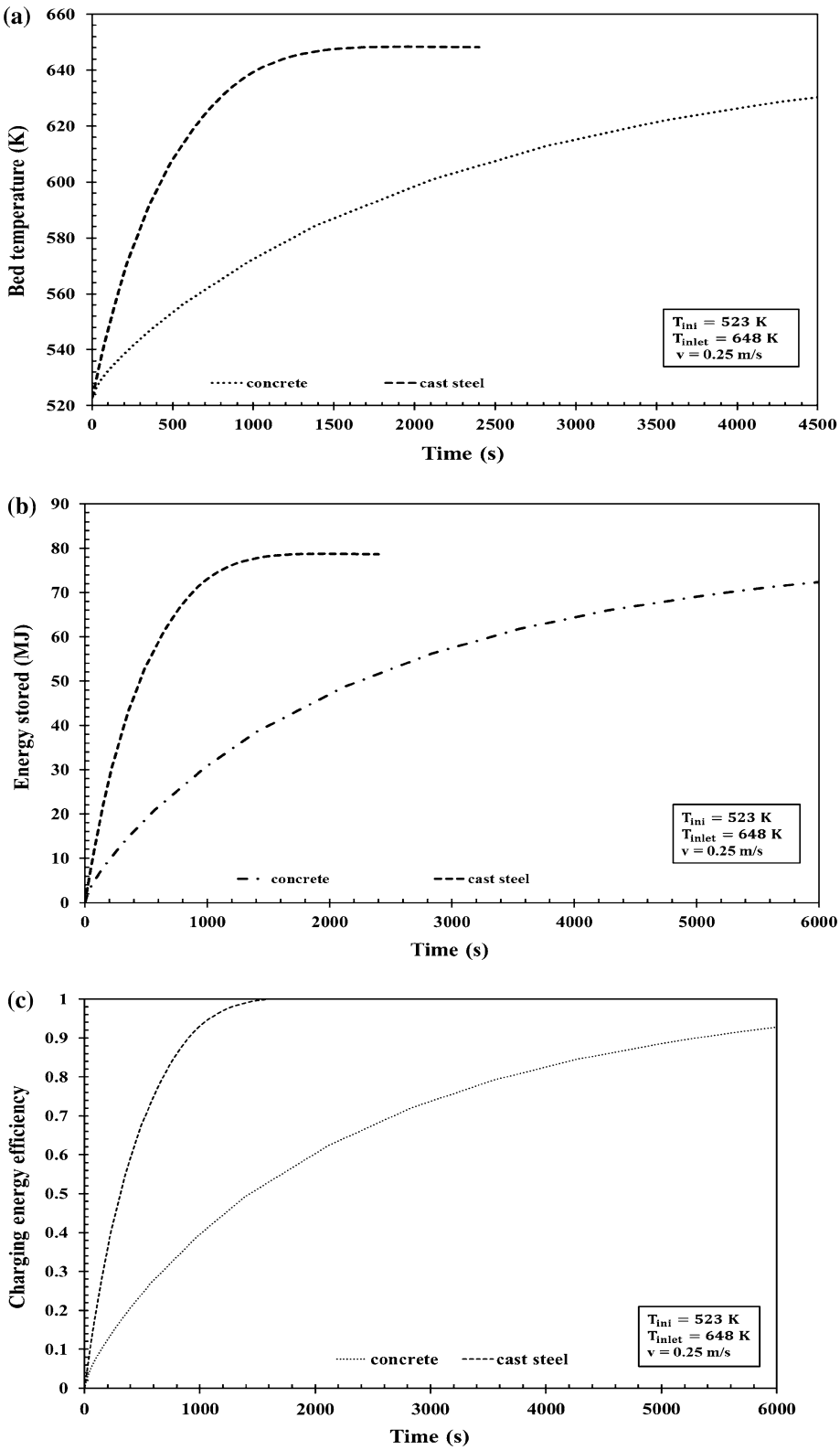

Fig. 7 Charging characteristics of concrete and cast steel beds **a** charging time, **b** rate of energy stored, **c** charging energy efficiency

Charging energy efficiency

The variation of charging energy efficiency of concrete and cast steel beds is illustrated in Fig. 7c. Charging energy efficiency of SHS bed is initially zero when the heat input is not given. Once the HTF is passed through the charging/discharging tubes, it increases due to the heat absorption from the HTF. This rate of increase in charging energy

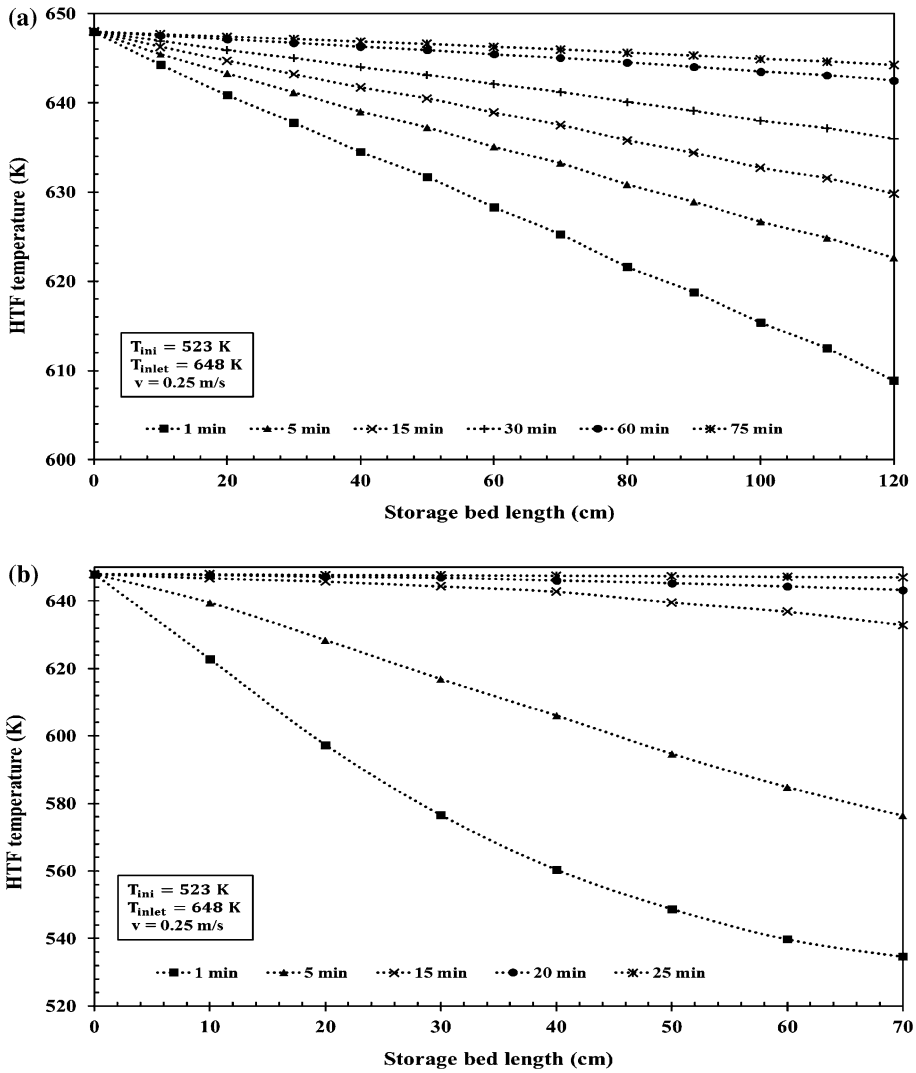

Fig. 8 Axial variation of HTF temperature during charging **a** concrete and **b** cast steel

efficiency for the cast steel SHS bed is higher than that of concrete bed. This is due to the higher rate of temperature increase in cast steel bed because of its high thermal conductivity. Since the charging energy efficiency is the function of volume average temperature of the storage bed, it varies in the same manner as the rate of charging of the SHS bed. The charging energy efficiency of concrete and cast steel SHS beds is 0.8 at their respective charging times.

Axial temperature variation in HTF during charging

In order to show the HTF temperature variation along the storage bed, HTF temperature is estimated along the length of the storage bed at a constant axial distance of 10 cm at different intervals of time, viz. 1, 5, 15, 30, 60 and 75 min for concrete bed shown in Fig. 8a and 1, 5, 15, 20 and 25 min for cast steel bed shown in Fig. 8b. The temperature drop of HTF is dominant during the initial period, and after certain time, its value is almost constant and no further drop in temperature is noticed as storage temperature itself rises with time, and as a result, the driving potential for conduction is retarded. The temperature drops of HTF are 39 K for concrete and 113 K for cast steel bed during 1 min of charging cycle. The temperature drop decreases with time, and its value is 3 K at 75 min of charging time for concrete bed, while for cast steel bed, the HTF outlet temperature approaches the inlet condition within 25 min of charging time.

Effects of HTF velocity on charging time

The effects of velocity of HTF on charging time for concrete and cast steel beds are shown in Fig. 9a, b, respectively. Increasing the HTF velocity increases the overall heat transfer coefficient enabling faster exchange of heat which reduces the charging time. For concrete and cast steel beds, the decrease in charging time of storage bed with HTF velocity of 0.25 m/s as compared to 0.1 m/s is higher than the decrease in charging time of storage bed

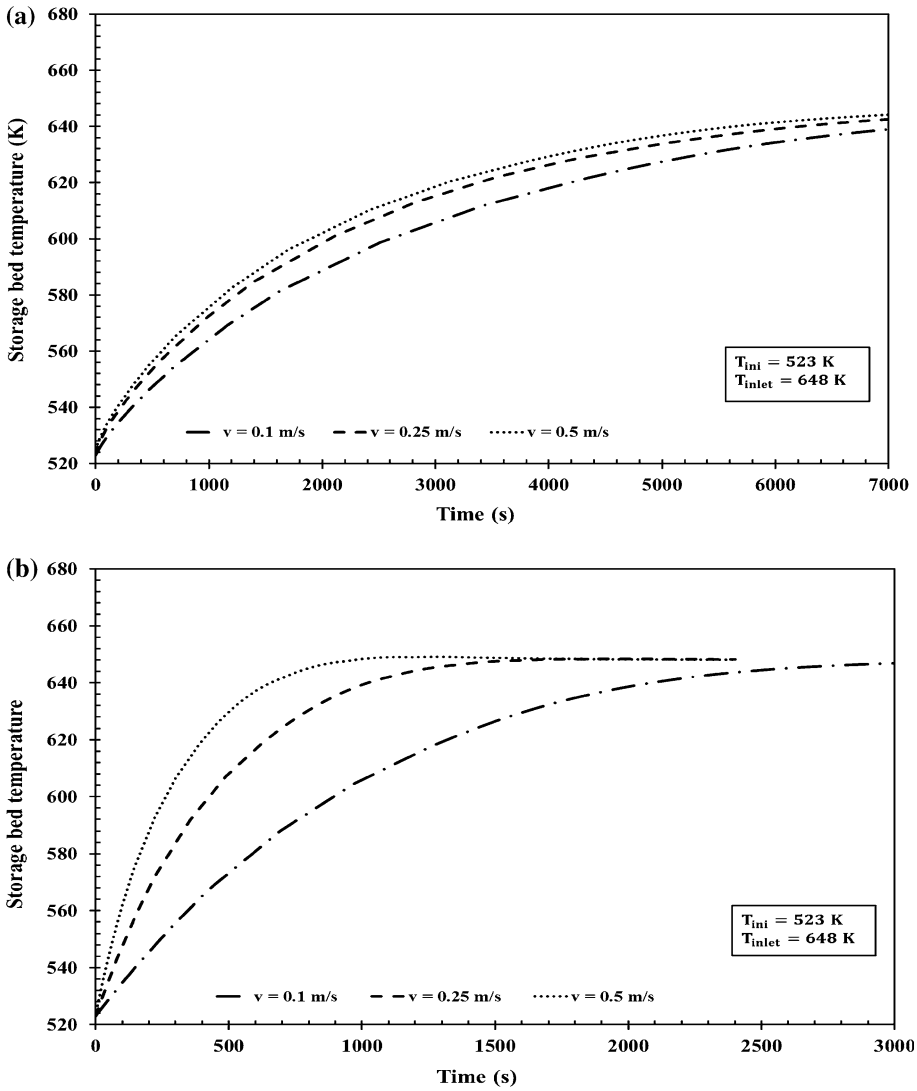

Fig. 9 Effects of HTF velocity on charging time **a** concrete and **b** cast steel

with HTF velocity of 0.5 m/s as compared to 0.25 m/s. It can be seen that increasing HTF velocity beyond 0.5 m/s will not have any significant reduction in the charging time. Charging time of concrete storage bed for HTF velocity of 0.1, 0.25 and 0.5 m/s are 4,493, 3,650 and 3,379 s, respectively, while for cast steel, the corresponding values are 1,400, 683 and 430 s.

Discharging time

Figure 10a shows the discharging time of concrete and cast steel storage beds. It can be noticed that the temperature drop of storage bed is rapid for first 7,200 s due to high driving potential for conduction and the slope of discharging curve becomes flat as the time progresses beyond 7,200 s. Therefore, 7,200 s can be taken as effective discharging time for concrete storage bed provided the energy recovered from the storage bed at 7,200 s is at least 50 MJ. Being high conductive material, cast steel reaches the inlet temperature of HTF in short time span and cast steel bed can be discharged completely. The complete discharging time of the cast steel bed is 1,820 s.

Thermal energy recovered

The rate of thermal energy discharged from concrete and cast steel storage bed is shown in Fig. 10b. The amount of thermal energy recovered from storage bed of different materials at their respective discharging time is calculated using Eq. 8. The thermal energy discharged is 59.78 MJ for concrete bed in an effective discharging time of 7,200 s, whereas cast steel storage bed discharges 62.75 MJ in complete discharging time of 1,820 s.

Discharging energy efficiency

Discharging energy efficiency of concrete and cast steel beds is presented in Fig. 10c. For cast steel SHS bed, it is about

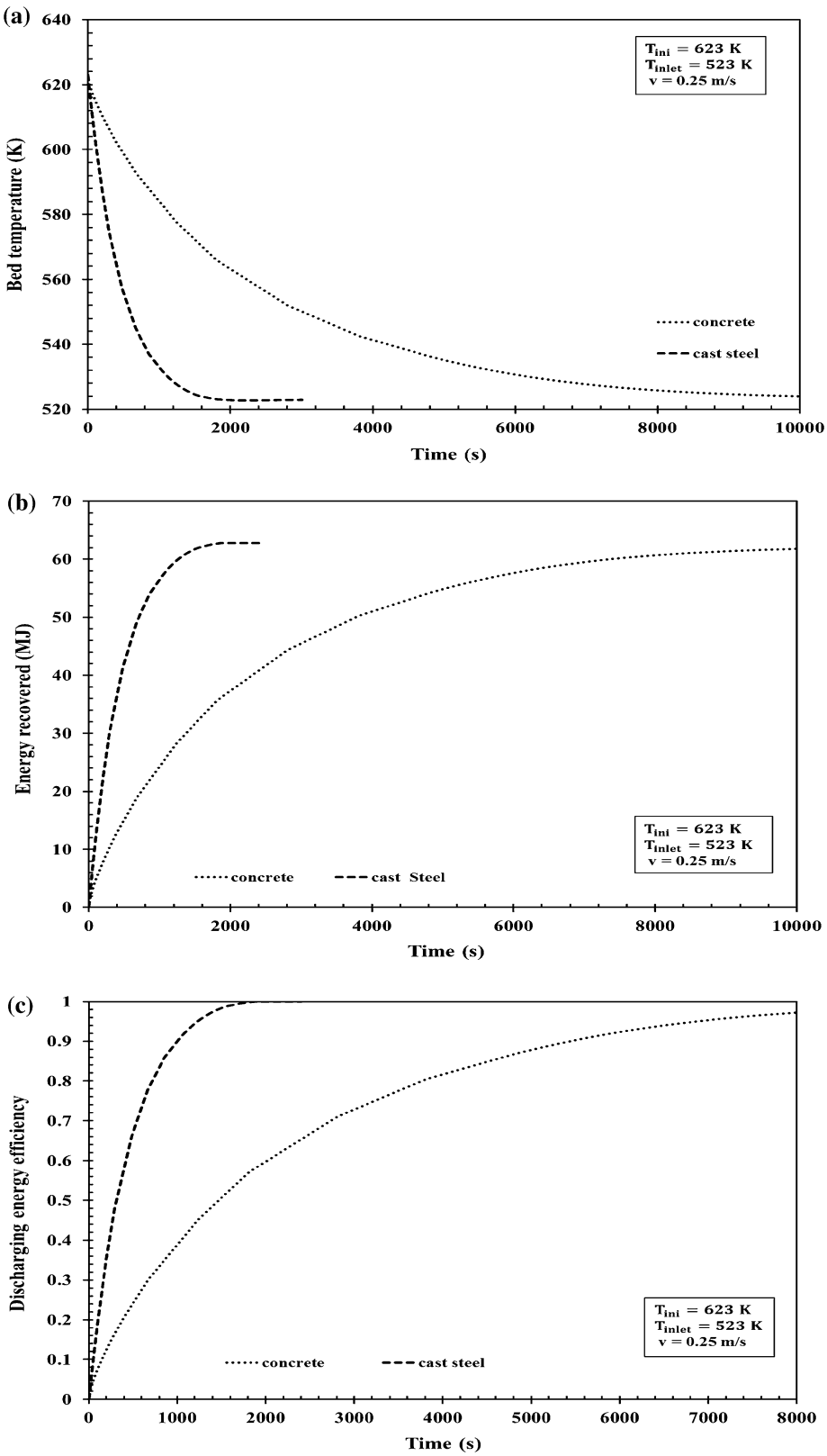

Fig. 10 Discharging characteristics of concrete and cast steel beds **a** discharging time, **b** rate of energy recovered and **c** discharging energy efficiency

100 % because the volume average temperature of cast steel SHS bed attains the value of inlet temperature within its discharging time, the average bed temperature does not reach the inlet temperature within the due to its low thermal conductivity. The discharging energy efficiency of concrete SHS bed is about 95.8 % at its discharging time of 7,200 s, as

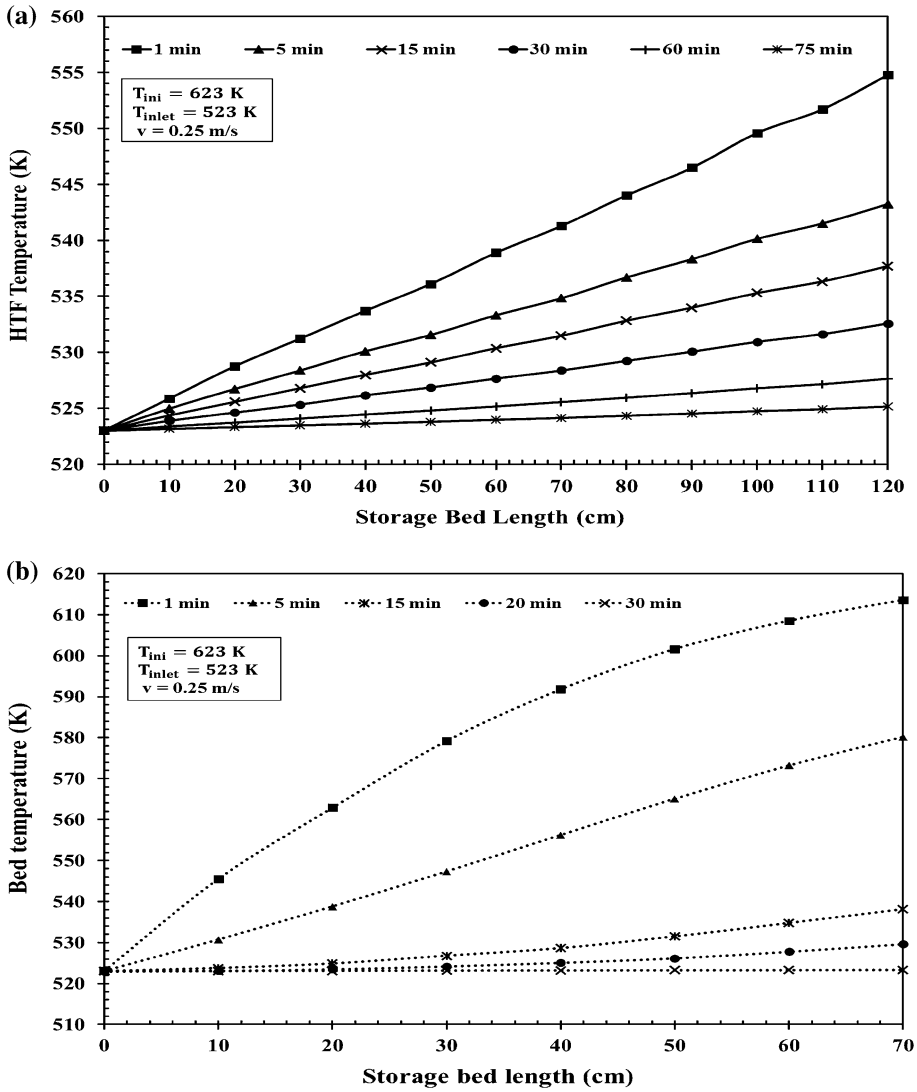

Fig. 11 Axial variation of HTF temperature during discharging **a** concrete and **b** cast steel

the average bed temperature does not reach the inlet temperature because of its low thermal conductivity.

Axial variation of HTF temperature during discharging

Discharging of charged storage bed is initiated by passing HTF at lower temperature of 523 K. HTF receives the heat from the charged storage bed resulting in the decrease of the storage bed temperature and increase of HTF temperature along the bed. It is seen from Fig. 11a, b that the temperature rise of HTF is dominant during the initial period of discharging time, and after certain duration, its value is almost constant. For example, during 1 min of discharging, the temperature rise of HTF is 31 K for concrete bed and 90 K for cast steel bed. The temperature rise decreases with time and its value is 2 K for 75 min of discharging time of concrete bed, while for cast steel bed, the HTF outlet temperature approaches the inlet condition within 30 min of discharging time.

Effects of HTF velocity on discharging time

The effects of velocity of HTF on discharging time for concrete and cast steel beds are shown in Fig. 12a, b, respectively. The discharging time of concrete storage bed for the HTF velocity of 0.1 m/s is 8,460 s and it decreases 14.89 % with 0.25 m/s and 15.13 % with 0.5 m/s HTF velocity. Thus, further increase in HTF velocity beyond 0.5 m/s will not change the results significantly. The discharging time for cast steel is 2,602 s with 0.1 m/s HTF velocity, and it decreases 30.10 % with 0.25 m/s and 56.30 % with 0.5 m/s HTF velocity.

Overall efficiency

The energy is degraded in the process of storage since it is extracted at a temperature lower than that it was previously stored. The overall efficiency of storage beds is evaluated using Eq. 9. Overall efficiency variation with bed

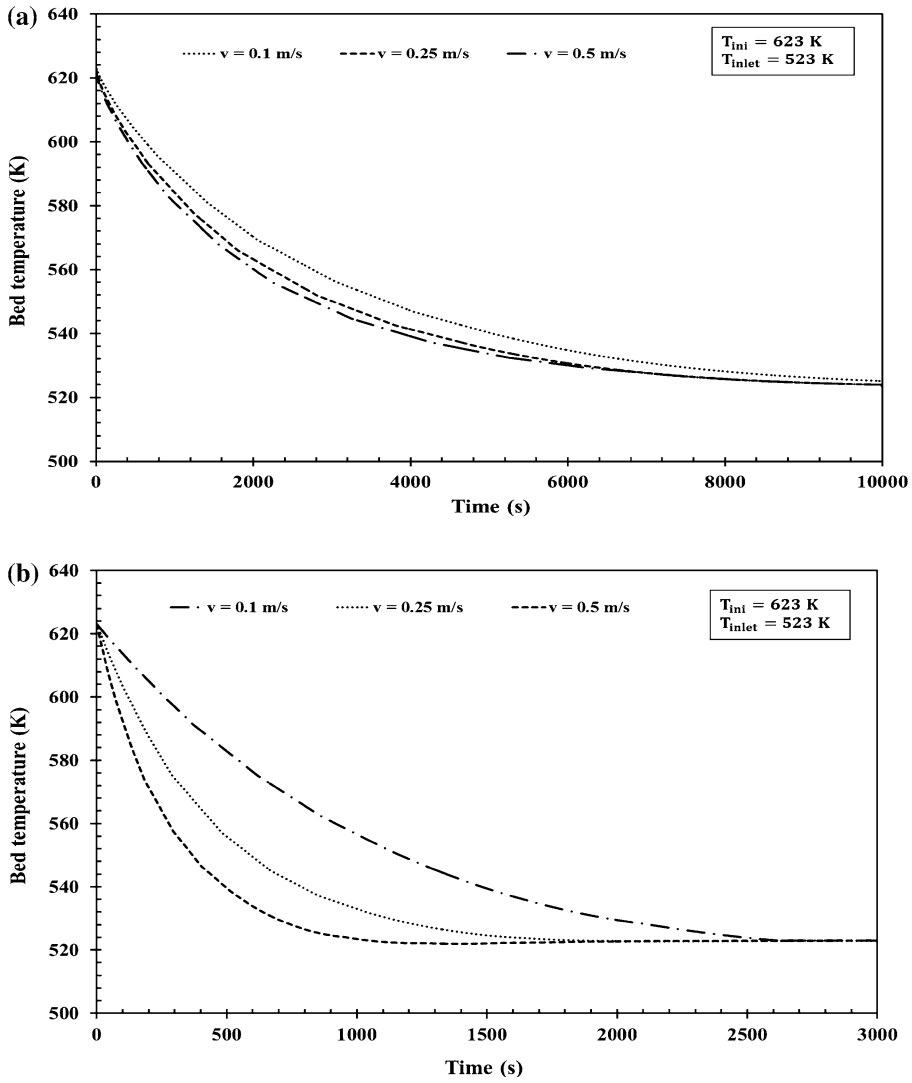

Fig. 12 Effects of HTF velocity on discharging time **a** concrete and **b** cast steel

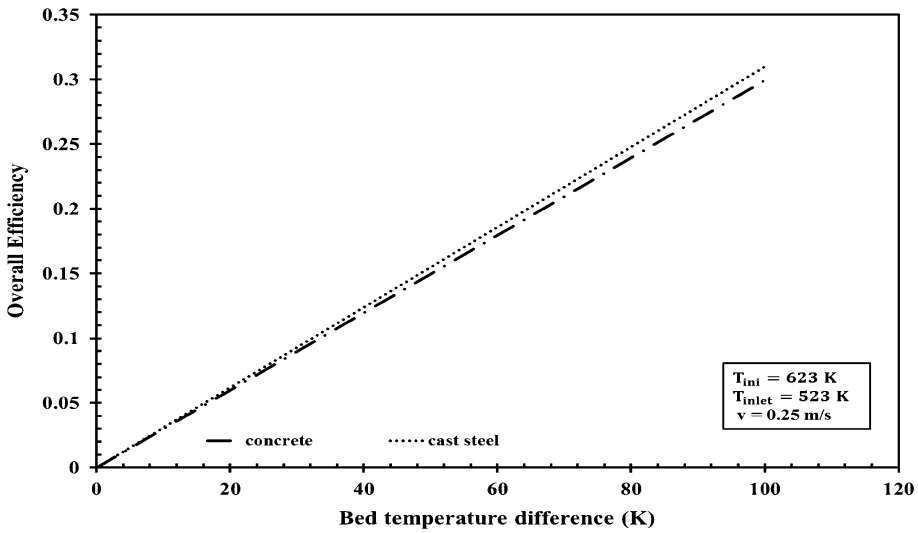

Fig. 13 Variation of overall efficiency with bed temperature difference

temperature difference during discharging cycle is shown in Fig. 13. Since concrete bed does not reach T_{inlet} (i.e. $\Delta T = 100$ K) during discharging, its overall efficiency is slightly lesser than cast steel bed. The overall efficiencies are 29.94 and 31 % for concrete and cast steel beds at their respective charging and discharging times.

Conclusions

Thermal models for predicting the charging and discharging characteristics of concrete and cast steel SHS units have been developed. The number of charging tubes has been optimized based on the charging time of the SHS bed. The predicted results matched well with the data reported in the literature. The charging and discharging time of concrete bed were much higher than that of cast steel bed. This suggests that concrete and cast steel bed can be used in line to reduce the overall charging and discharging time of industrial scale SHS system. The axial variation of HTF during the charging and discharging of SHS beds were analysed. The effect of HTF velocity on charging and discharging time of storage beds has been analysed, and it was observed that the charging and discharging time can be reduced significantly by increasing the HTF velocity up to certain limits (0.5 m/s). For cast steel bed, the increase in HTF velocity resulted in the proportional reduction in charging/discharging time, while these effects in concrete were less because of its low thermal conductivity.

Acknowledgments The authors sincerely thank the Department of Science and Technology (DST), Government of India, for their financial support [Project No: DST/TM/SERI/2K10/53(G)].

References

Anderson R, Shiri S, Bindra H, Morris JF (2014) Experimental results and modeling of energy storage and recovery in a packed bed of alumina particles. Appl Energy 119:521–529. doi:10.1016/j.apenergy.2014.01.030

Gil A, Medrano M, Martorell I, Cabeza F (2010) State of the art on high temperature thermal energy storage for power generation. Part 1—concepts, materials and modellization. Renew Sust Energy Rev 14:31–55. doi:10.1016/j.rser.2009.07.035

Haller MY, Cruickshank C, Streicher W, Harrison SJ, Andersen E, Furbo S (2009) Methods to determine stratification efficiency of thermal storage processes–review and theoretical comparison. Sol Energy 83:1847–1860. doi:10.1016/j.solener.2009.06.019

John EE, Hale WM, Selvam RP (2011) Development of a high performance concrete to store thermal energy for concentrating solar power plants. In: Proceedings of the ASME 2011 5th international conference on energy sustainability, Washington, USA. http://itme000.louisiana.edu/assign/Solar%20Thermal%20Project/Literature

Khare S, Knight C, McGarry S (2013) Selection of materials for high temperature sensible energy storage. Sol Energy Mater Sol Cells 115:114–122. doi:10.1016/j.solmat.2013.03.009

Laing D, Steinmann W, Tamme R, Richter C (2006) Solid media thermal storage for parabolic trough power plants. Sol Energy 86:1283–1289. doi:10.1016/j.solener.2006.06.003

Miró L, Navarro ME, Suresh P, Gil A, Fernández AI, Cabeza LF (2014) Experimental characterization of a solid industrial by-product as material for high temperature sensible thermal energy storage (TES). Appl Energy 113:1261–1268. doi:10.1016/j.apenergy.2013.08.082

Nandi BR, Bandyopadhyay S, Banerjee R (2012) Analysis of high temperature thermal energy storage for solar power plant. In: Proceedings of the third IEEE International conference on sustainable energy technologies, Kathmandu, Nepal. doi:10.1109/ICSET.2012.6357438

Sragovich D (1989) Transient analysis for designing and predicting operational performance of a high temperature thermal energy storage system. Sol Energy 43:7–16. doi:10.1016/0038-092X(89)90095-9

Tamme R, Laing D, Steinmann W (2004) Advanced thermal energy storage technology for parabolic trough. J Sol Energy-T ASME 126:794–800. doi:10.1115/1.1687404

Tian Y, Zhao CY (2013) A review of solar collectors and thermal energy storage in solar thermal applications. Appl Energy 104:538–553. doi:10.1016/j.apenergy.2012.11.051